Choice of Tuning Parameters on 3D IC Engine Simulations Using G-Equation

Author, co-author (Do NOT enter this information. It will be pulled from participant tab in MyTechZone)

Affiliation (Do NOT enter this information. It will be pulled from participant tab in MyTechZone)

Abstract

3D CFD spark-ignition IC engine simulations are extremely complex for the regular user. Truly-predictive CFD simulations for the turbulent flame combustion that solve fully coupled transport/chemistry equations may require large computational capabilities unavailable to regular CFD users. A solution is to use a simpler phenomenological model such the G-equation that decouple transport/chemistry result. Such simulation can still provide acceptable and faster results at the expense of predictive capabilities. While the G-equation is well understood within the experienced modeling community, the goal of this paper is to document some of them for a novice or less experienced CFD user who may not be aware that a phenomenological models of turbulent flame combustion usually require heavy tuning and calibration from the user to mimic experimental observations. This study used ANSYS® Forte, Version 17.2, and the built-in G-equation model, to investigate two tuning constants that influence flame propagation in 3D CFD SI engine simulations: the stretch factor coefficient, C_{ms} and the flame development coefficient, C_{m2}. After identifying several C_{m2}-C_{ms} pairs that matched experimental data at one operating conditions, simulation results showed that engine models that used different C_{m2}-C_{ms} sets predicted similar combustion performance, when the spark timing, engine load, and engine speed were changed from the operating condition used to validate the CFD simulation. A dramatic shift was observed when engine speed was doubled, which suggested that the flame stretch coefficient, C_{ms}, had a much larger influence at higher engine speeds compared to the flame development coefficient, C_{m2}. Therefore, the C_{m2}-C_{ms} sets that predicted a higher turbulent flame under higher in-cylinder pressure and temperature increased the peak pressure and efficiency. This suggest that the choice of the C_{m2}-C_{ms} will affect the G-equation-based simulation accuracy when engine speed increases from the one used to validate the model. As a result, for the less-experimented CFD user and in the absence of enough experimental data that would help retune the tuning parameters at various operating conditions, the purpose of a good G-equation-based 3D engine simulation is to guide and/or complement experimental investigations, not the other way around. Only a truly-predictive simulation that fully couples the turbulence/chemistry equations can help reduce the amount of experimental work.[1]

Introduction

3D CFD engine simulation packages are used to guide and/or complement experimental investigations, and to provide in-cylinder details that conventional data acquisition methods cannot capture [1, 2]. 3D CFD IC engine simulations in the literature [3-5] combine complex phenomenological sub-models with solution-adaptive mesh refinement and coarsening [6, 7], and improved chemistry solvers [8, 9]. The goal is to accurately predict results with minimum computational costs and reasonable running times.

3D CFD packages use simple or complex models to describe the turbulent flame combustion inside a spark-ignition (SI) engine. Most of the commercial software allow the user to choose the degree of complexity of these models based on the time required to run the simulation and computational cost. Subsequently, the simulation can be more phenomenological-in-nature when heavy tuning and calibration are required from the user to mimic experimental observations or they can be truly predictive if the models solve fully coupled transport/chemistry equations. As a result, as complex models may require large computational capabilities unavailable to regular CFD users, a simpler model can still provide acceptable and faster results at the expense of predictive capabilities. One such option that decouples the transport/chemistry equations is the G-equation [10], which uses a scalar field approach to describe the flame position. More details about the G-equation are presented in the *Combustion Model Theory* section.

While references [10-22] detail the G-equation theory, no reference in the open literature provides a *complete* explanation of its application in a premixed-combustion IC engine simulation. As a result, while the G-equation concepts and limitations described in this paper are well understood within the experienced modeling community, the goal of this paper is to document some of them for a novice or less experienced CFD user. For example, compared to a truly-predictive model, the G-equation employs several important tunable constants to calibrate flame sub-models and improve the

accuracy. However, not all software developers are implementing the G-equation the same. Specifically, the developer may use additional tuning parameters to improve simulation accuracy. The reason is that in addition to engine geometry effects, the combustible mixture and flame properties can affect the model accuracy, especially when reduced chemistry is used. While the software specifies the range of each tunable constant, the user chooses their values based on how well the simulation matches experimental data at some operating condition(s). Once these tunable constants are determined, the simulation intent is to predict in-cylinder pressure and heat release rate over different operating conditions without the need to modify the tuning values for each set of operating conditions (i.e., there is a unique set that would simulate most of the engine operation) [6], even if the G-equation does not solve fully coupled turbulence/chemistry interaction. While an experienced CFD user knows that a non-predictive model cannot cover a wide operating range without retuning at various operating, a less experienced CFD user can expect that the G-equation-based simulation (i.e., a phenomenological model) can *replace* rather than *guide* experimental investigations and engine development. While this may be true for truly-predictive 3D simulations that solve fully coupled turbulence/chemistry equations, the goal of this study was to show the limitations of such expectations when using a simplified model based on the G-equation. Specifically, this study investigated several G-equation tuning constants that were selected based on their influence on premixed-combustion flame propagation in SI engines, which is discussed in the combustion theory section. The objectives were to first match experimental pressure trace and heat release data at one operating condition using different sets of tuning constants, then to investigate if each set of tuning constants would predict a different simulation outcome when engine operating conditions such as speed, load, or spark timing were changed. In-cylinder phenomena was predicted in this study using a CFD software package specifically designed for IC engines simulations (ANSYS® Forte, Version 17.2) and the built-in G-equation model. However, similar 3D CFD IC engine software (e.g., Convergent Science' Converge CFD) also includes the G-equation model and, while not exactly the same, similar tuning coefficients.

Combustion Model Theory

This section describes the G-equation-based combustion model used in ANSYS® Forte, a phenomenological model using tuning and calibration to mimic experimental observations, but the discussion applies to any similar CFD packages that use the G-equation. The G-equation in ANSYS® Forte combines two main sub-models to simulate the turbulent flame premixed combustion inside a spark-ignition (SI) engine: the spark kernel model and the turbulent combustion model [4, 6, 7, 11, 12]. The next subsection presents a summary of the G-equation model theory, including a description of the important tuning constants used.

The G-Equation-Based Turbulent Premixed Combustion Model

The *G*-equation model [10, 12] predicts in-cylinder turbulent flame combustion without including chemistry source terms in the transport equations [13]. The *G* term is the scalar distance between the instantaneous and the mean flame front [12]. The *G*-equation model uses Eqns. 1 and 2 and the Favre averaging method to output the turbulent flame front location and flame brush thickness, respectively:

$$\frac{\partial \tilde{G}}{\partial t} + \left[\widetilde{(\vec{u})} - \tilde{u}_{vertex}\right] \cdot \nabla \tilde{G} = \frac{\bar{\rho}_u}{\bar{\rho}_b} S_T^0 \left|\nabla \tilde{G}\right| - D_T \tilde{\kappa} \left|\nabla \tilde{G}\right| \quad (1)$$

$$\frac{\partial \tilde{G}''^2}{\partial t} + \widetilde{(\vec{u})} \cdot \nabla \tilde{G}^{n^2} = \nabla_{\|} \cdot \left(\frac{\bar{\rho}_u}{\bar{\rho}_b} D_T \nabla_{\|} \tilde{G}''^2\right) + 2 D_T \left(\nabla \tilde{G}\right)^2 - C_s \frac{\tilde{\varepsilon}}{\tilde{k}} \tilde{G}''^2 \quad (2)$$

where, $\vec{u}$ and $\vec{u}_{vertex}$ are fluid and moving vertex velocity, respectively, $\bar{\rho}_u$ and $\bar{\rho}_b$ are the average densities for unburned and burned gas, respectively, S_T^0 is the turbulent flame speed, D_T is the turbulent diffusivity, $\nabla_{\|}$ is the tangential gradient operator, $C_s\left(\tilde{\varepsilon}/\tilde{k}\right)\widetilde{G''^2}$ is the sum of Favre kinematic restoration and Favre scalar dissipation (i.e., the dominant term in corrugated flamelets regime and the dominant term in thin reaction zones regime) [12], $\tilde{k}$ and $\tilde{\varepsilon}$ are the Favre mean turbulence kinetic energy and its dissipation rate from the RNG k-ε model [23], C_s is a modeling constant derived from spectral closure [17], and $\tilde{\kappa}$ is the Favre mean flame front curvature, defined as [17]:

$$\tilde{\kappa} = \nabla\left(\nabla \tilde{G} / \left|\nabla \tilde{G}\right|\right) \quad (3)$$

Predictions of the turbulent flame speed are needed to solve the G-equation model. The unsteady turbulent flame speed is derived from the mean gradient, defined as the flame surface area ratio [12, 17]:

$$\frac{S_T^0}{S_L^0} = 1 + I_P \cdot \left[-\frac{a_4 b_3^2}{2b_1}\frac{l_I}{l_F} + \sqrt{\left(\frac{a_4 b_3^2}{2b_1}\frac{l_I}{l_F}\right)^2 + a_4 b_3^2 \frac{u'}{S_L^0}\frac{l_I}{l_F}}\right] \quad (4)$$

where, S_L^0 (laminar flame speed) is calculated using a power-law formulation [18, 19] or interpolated from flame speed tables, l_I is the turbulence integral length scale (calculated from the RNG k-ε model), l_F is the laminar flame thickness, b_1 (a major tuning parameter) is the ratio of fully-developed turbulent flame speed to the turbulence velocity (a.k.a. the turbulent flame speed ratio) [11], a_4 and b_3 are modeling constants, and u' is the turbulence intensity/velocity. The progress variable I_P is defined as:

$$I_P = \sqrt{1 - exp\left(-c_{m2}\frac{t - t_0}{\tau}\right)} \quad (5)$$

The exponentially increasing term I_P controls the effects of the ignition kernel flame turbulence on the early flame development (i.e., during the transition from laminar to turbulent flame) [13]. The value of I_P should equal unity for a fully developed turbulent flame. The flame development coefficient C_{m2} in Eq. 5 is a derived from the modeling constant C_s [11, 17]. The simulation uses C_{m2} as a tuning coefficient to minimize model uncertainties, including mesh resolution effects [13, 17].

The turbulent flame brush thickness, $l_{F,t}$, is derived from Eq. 2 [12]:

$$l_{F,t} = \left.\frac{\sqrt{\tilde{G}''^2}}{\left|\nabla \tilde{G}\right|}\right|_{\tilde{G}=G_0} = b_2 l_I I_P \quad (6)$$

where, b_2 is a constant equal to 1.78 from dimensional analysis.

The G-equations, the Reynolds-Averaged Navier Stokes (RANS) equations, and the Re-normalized group (RNG) k-ε model constitute a closed set of equations that completely describe the turbulent flame propagation [13]. The resulting flame front information is then used

to calculate in-cylinder heat release, end gas kinetics, and emissions formation [11, 13].

The two main tuning constants that need calibrated in the *G*-equation model are the turbulent flame speed ratio, b_1 and flame development coefficient, C_{m2} (the latter needed only when a spark exists). A larger b_1 increases the magnitude of fully-developed turbulent flame speed, which in turn can increase flame propagation. C_{m2} controls the speed of transition from laminar to fully developed turbulent flame. Specifically, a larger C_{m2} accelerates the transition to a fully developed turbulent flame.

Spark Kernel Sub-Model

The discrete particle ignition kernel (DPIK) flame model, based on Lagrangian particles [20], was introduced because the numerical grid sizes or time steps are not always small enough to meet the requirements of describing ignition phenomena at the spark plug and the subsequent flame kernel development [21]. The kernel growth rate can be derived from mass conservation and ideal gas law [see 15 for details]:

$$\frac{dr_k}{dt} = \frac{\rho_u}{\rho_k}\left(S_{plasma} + S_T\right) \tag{7}$$

where, r_k is the spark kernel radius, ρ_u and ρ_k are gas density for local unburned mixture and inside the kernel volume, respectively, S_{plasma} is the plasma velocity, and S_T is the turbulent flame speed.

Assuming a spherical ignition kernel, the spark discharge energy can be used to calculate plasma velocity [17]:

$$S_{plasma} = \frac{\dot{Q}_{spk}\eta_{eff}}{4\pi r_k^2\left[\rho_u(u_k - h_u) + P\frac{\rho_u}{\rho_k}\right]} \tag{8}$$

where, $\dot{Q}_{spk}$ is the electrical energy discharge rate, η_{eff} is electrical energy transfer efficiency that accounts for electrode heat loss and plug geometry [15]; h_u is the unburned gas enthalpy, u_k is the internal energy of the kernel mixture, and P is the local pressure. The turbulent flame speed at the spark kernel, S_T, is defined as [15, 22]:

$$\frac{S_T}{S_L^0} = I_0 + \sqrt{I_0}\cdot\sqrt{\frac{u'}{u'+S_L^0}}\cdot\sqrt{1-\frac{1}{e^{\left(\frac{r_k}{l_I}\right)}}}\cdot\sqrt{1-\frac{1}{e^{\left[\frac{t}{l_I}(u'+S_L^0)\right]}}}\cdot\left(\frac{u'}{S_L^0}\right)^{\frac{5}{6}} \tag{9}$$

where, I_0 is the stretch factor affecting on the kernel development, the second, third, and fourth radical expressions on the RHS are the effective turbulence factor, the size dependent integral length scale, and the time dependent integral time scale, respectively [22], and $(u'/S_L^0)^{5/6}$ a term that accounts for fully developed turbulent combustion [22]. I_0 can be calculated with Eq. 10 [22]:

$$I_0 = 1 - \left[\left(\frac{l_F}{15l_I}\right)^{\frac{1}{2}}\left(\frac{u'}{S_L^0}\right)^{\frac{3}{2}} + 2\frac{l_F}{r_k}\frac{\rho_u}{\rho_k}\right]\cdot\left[\frac{1}{Le} + \left(\frac{Le-1}{Le}\right)\frac{T_a}{T_{ad}}\right] \tag{10}$$

where, Le is the Lewis number, and T_a and T_{ad} are activation and adiabatic flame temperatures, respectively. If Lewis number is less than one, the stretch factor would be larger than unity and thus the turbulent flame speed increases. However, this would happen for rich mixtures only, which is not always the case in stoichiometric SI engine combustion [22]. If Lewis number equals one, the last term on the RHS of Eq. 10 is also equal to 1, which simplifies the stretch factor equation to [12]:

$$I_0 = 1 - \left(\frac{l_F}{15l_I}\right)^{\frac{1}{2}}\left(\frac{u'}{S_L^0}\right)^{\frac{3}{2}} - 2\frac{l_F}{r_k}\frac{\rho_u}{\rho_k} \tag{11}$$

The 2nd and 3rd terms on the RHS in Eq. 11 represent contributions from the turbulent strain and the kernel geometrical curvature, respectively [13].

$$I_0 = 1 - C_{ms}\cdot\left(\frac{l_F}{15l_I}\right)^{\frac{1}{2}}\left(\frac{u'}{S_L^0}\right)^{\frac{3}{2}} - 2\frac{l_F}{r_k}\frac{\rho_u}{\rho_k} \tag{12}$$

Equation 12, which calculates the flame stretch factor in ANSYS Forte, introduces a flame stretch factor coefficient, C_{ms}, as a tunable constant, probably to compensate for other sub-model uncertainties. It is important to mention that the G-equation model in Converge CFD does not use a flame stretch factor coefficient (i.e., $C_{ms} = 1$).

It is noteworthy that the G-field is also established during the simulation of the spark kernel mode, using the positions of the kernel particles. The G-field provides data for chemical heat release calculations [11]. Equation 13 [11] shows the transition criterion from spark kernel model to turbulent flame combustion model:

$$r_k \geq C_{m1}\cdot l_I = C_{m1}\cdot 0.16\cdot\frac{k^{1.5}}{\varepsilon} \tag{13}$$

where, C_{m1} is the kernel-flame-to-G-equation switch constant, always equal to 2.0.

The initial kernel radius $r_{k,initial}$ is a model constant defined by the user. The stretch factor coefficient, C_{ms}, has a large influence on the spark kernel development in the spark kernel model. If the stretch factor coefficient is increased, a slower flame kernel propagation results.

It is expected that the choice of various constants in Eqns. 4, 5, and 12 will affect simulation results. Specifically, the stretch factor coefficient, C_{ms}, and the flame development coefficient, C_{m2}, control the early flame development. After the early flame established, the turbulent flame speed ratio, b_1, controls the fully-developed turbulent flame speed. As both C_{ms} and C_{m2} control early flame development, the objective of present study is to find C_{m2}-C_{ms} sets that match experimental data at a specific engine operating condition and constant b_1, then change operating conditions (i.e., different engine speed and load) and compare predictions. As the user should use the same CFD model/sub-model setup across all possible engine operating conditions [6, 7], it is expected that the choice of C_{m2}-C_{ms} values would not affect model predictions, in turn not affecting the simulation accuracy across the engine operating range.

Experimental Setup

Engine experiments were performed in a 2.0-L GDI engine (GM, Model Ecotec LNF) at Oak Ridge National Laboratory's National Transportation Research Center. Reference [24] describes the experimental setup in detail. Table 1 shows engine specifications. Experimental data shown here is from cylinder 1 of a 4-cylinder engine. The combustion chamber geometry and camshaft profiles were unchanged from the stock configuration.

Table 1. Engine specifications

Cycle	4-stroke SI
Bore [mm] × Stroke [mm]	86 × 86
Displacement [liters]	2.0
Intake valve open	67º BTDC exhaust
Intake valve close	127º BTDC compression
Exhaust valve open	106º ATDC compression
Exhaust valve close	30º ATDC exhaust
Connecting rod length [mm]	145.5
Wrist pin offset toward	0.8
Compression ratio	9.2:1

The engine was equipped with the production side-mounted, direct-injection fueling system. This system injects the fuel early in the intake stroke. Table 2 presents the engine operating conditions including fuel injection details. References [25, 26] describe the injection individual jet direction and dimensions.

Table 2. Engine operating conditions

Engine speed [rpm]	2000
Intake manifold pressure [kPa]	50
Intake air temperature [ºC]	27
Spark timing	23º BTDC compression
Fuel	Iso-Octane
SOI	280º BTDC compression
Injection duration [ms]	1.02
Injection pressure [bar]	100
Fuel mass [mg/cycle]	16
Equivalence ratio	1.0
Number of nozzle holes and diameter [mm]	6 × 0.23 [25]

Numerical Model

The combustion chamber's 3D model included the intake and exhaust ports. A reduced gasoline surrogate mechanism (Lawrence Livermore National Laboratory, [27, 28]) consisting of 312 species and 1488 elementary reactions simulates the fuel. As the fuel was injected very early in the intake stroke in the engine experiments and no soot emissions were observed, the CFD model assumed fully premixed fuel and air entering the intake runner boundary of the simulation grid. As a result, intake boundary conditions were slightly modified to account for the additional fuel mass flowing though the intake port compared to air only in the engine experiments. This approach did not capture the effects of in-cylinder fuel stratification associated with direct fuel injection or the changes in in-cylinder turbulence from the evaporating spray, even if the injection event took place early in the intake stroke. This can possibly create large differences in terms of flame inception, propagation, and emissions between the experiments and simulations. However, to reduce the time and cost of the simulation and in the absence of correct injector information (i.e., nozzle size and orientation, etc.) the authors considered that a simple premixed combustion model would avoid the inclusion of the additional spray model uncertainty during the simulation analysis. Consequently, the CFD model did not include a spray model. The CFD simulation used a RANS approach [6, 7] with a RNG k-ε model [23, 29] that was specifically designed to simulate in-cylinder

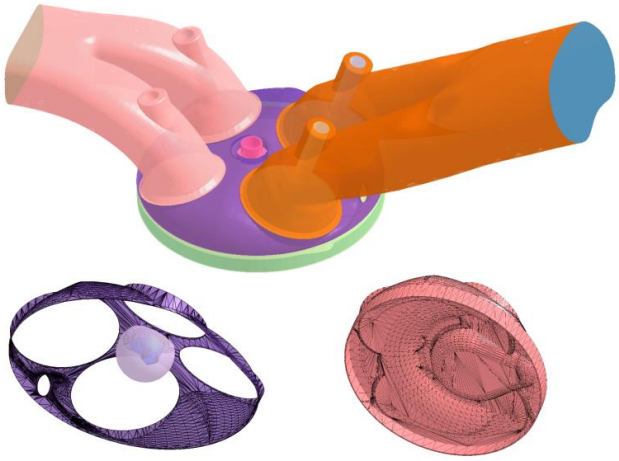

Figure 1. Model 3D mesh. The ball around the spark plug location identifies the refined meshing zone.

turbulent compressible flows. Other main sub-models include the G-equation combustion model, the discrete particle ignition kernel flame model, and the flame quenching model. The local flame speed was calculated from software's existing iso-octane laminar flame speed table. The initial gas mixture defined in-cylinder residual gas composition and the simulation started at the opening of the exhaust valve. Automatic mesh generation generated meshes that changed with piston position. Figure 1 shows the combustion chamber model and mesh at the top dead center (TDC). While the global mesh size was 3.5mm, the software refined the mesh at the spark plug, boundary layers, valves and crevice locations. Specifically, Figure 1 shows that spark plug location was refined by creating a 10 mm ball around the spark plug using a mesh size of one quarter of the global size.

Results

Several subsections present and discuss the numerical results. The first subsection identified several sets of values for the flame development coefficient and stretch factor coefficient that can be used to match the average experimental pressure trace and heat release data at one operating condition. As the combined effects of the two tuning constants on the turbulent flame behavior were not linear, the next subsection shows the results of a parametric study that observed the individual effects of each tuning constant. Finally, a parametric study that changed the spark timing, the engine load and speed was performed for three different sets tuning parameters identified before. The parametric study did not change the boundary conditions (e.g., wall temperature) to avoid including any additional effects.

Model Validation

The differences in air-fuel mixing between the experiments (GDI) and simulation (premixed combustion) can result in different flame inception and propagation, efficiency, and emissions between the experiments and simulations. As a result, the GDI experimental data was only used to calibrate the CFD model. The combustion theory and literature [6, 13] mention b_1 (the turbulent flame speed ratio in Eq. 4) as the primary tunable constant, with a suggested range of values of 1.5-3. However, the experimental data could not be matched data by manipulating b_1 only (i.e., without choosing

appropriate values for the flame development coefficient, C_{m2}, and the stretch factor coefficient, C_{ms}, too). Following the suggested range of values for C_{ms} and C_{m2} of 0.5-2.5 and 0-1, respectively, a parametric study manipulated b_1, C_{ms}, and C_{m2} until a set of constants produced simulation results that matched the experiment pressure trace and heat release. This set of constants is identified as *Sim1* in the rest of the paper. Table 3 and Figs. 2a and 2b show that *Sim1* matched reasonably well the experimental pressure trace, apparent heat release rate (AHRR), as well as some of the main combustion parameters such as in-cylinder maximum pressure and its location, start of combustion (SOC), end of combustion (EOC), combustion duration, and indicated thermal efficiency (η_{th}). Table 3 shows that the model predicted lower CO and HC emissions. However, while the CO emissions were on a similar order of magnitude with experimental data, the HC emissions in the experiment were a couple of orders of magnitude higher than those predicted by the simulations, which reduced the experimental IMEP in Table 3. As mentioned, the simulation considered a homogeneous gas mixture compared to the stratified charge in the real engine, which would affect CO or HC emissions. In addition, the mechanism used to simulate the fuel combustion (i.e., LLNL's gasoline surrogate mechanism, which was assembled from existing LLNL mechanisms for n-heptane, iso-octane, toluene, and C5-C6 olefins) may affect the emission predictions when the fuel consists of iso-octane only, as in this study. But this work did not focus on comparing predicted emissions with experimental data. The predicted emissions were only used to complement the pressure-based analysis between simulations. Furthermore, the model did not include NO_x formation, therefore there are no predictions for the NO_x emissions.

After identifying the b_1, C_{ms}, and C_{m2} that matches the experimental data, a parametric study that kept b_1 constant identified two more C_{m2}-C_{ms} sets that predicted similar results. These two set of constants are identified as *Sim2* and *Sim3* in the rest of the paper. Table 4 shows the values for these three b_1, C_{ms}, and C_{m2} sets.

Table 3. Main combustion parameters for the experimental data and the numerical simulations. The percentages indicate the change from *Sim1*.

Experiment/ Simulation #	Exp	*Sim1*	*Sim2*	*Sim3*
IMEP [bar]	4.6	5.2	5.2	5.2
Maximum Pressure [bar]	24.0	24.8	24.2	24.3
Location P_{max} [CA]	16.6	17.1	18.1	18.0
CA10 [CA ATDC]	-0.2	-1.9	-1.4	-1.5
CA50 [CA ATDC]	10.4	11.0	11.5	11.6
CA90 [CA ATDC]	25.8	27.6	28.0	27.5
Maximum Temp [K]	N/A	2372	- 0.3%	- 0.1%
Max-Temp Location [CA]	N/A	26.5	27.5	27.5
Combustion Duration [CA D]	26.0	29.5	29.5	29.0
Indicated η_{th} [%]	32.4	37.1	37.0	37.0
CO Emission [g/kW-hr]	49.2	13.7	+2.2%	+1.9%
HC Emission [g/kW-hr]	2.77	0.008	-1.2%	-31.7%

Table 4. Tuning constants values

Validated Model	b_1	C_{ms}	C_{m2}
Sim1	2.5	1.0	2.5
Sim2	2.5	0.5	1.8
Sim3	2.5	0.0	1.5

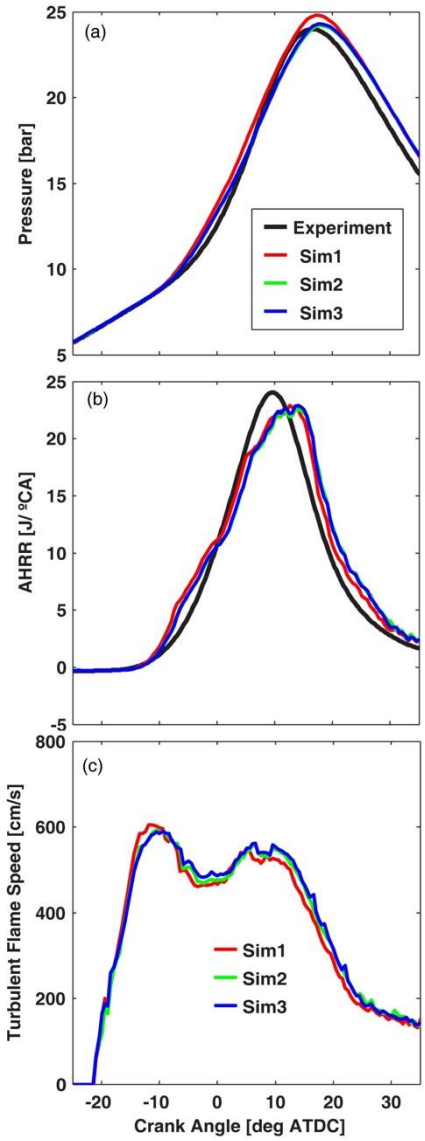

Figure 2. Pressure trace, apparent heat release rate (AHRR), and turbulent flame speed (simulations only) for experiment and numerical simulations. The transition from DPIK to G-equation was at -19 CAD ATDC.

More, Table 3 and Figs. 2a and 2b show that *Sim2* and *Sim3* also matched reasonably well the experimental pressure trace, AHRR, as well as some of the main combustion parameters. Combustion duration in table 3 was defined as the difference between the CA10 and CA90, which are the crank angle corresponding to 10% and 90% heat release. In addition, Table 3 and Fig. 3 show minimum differences between *Sim1*, *Sim2* and *Sim3*, including differences in the in-cylinder maximum temperature and its location, and the CO and HC emissions (the large percentage difference in HC emissions between *Sim 1* and *Sim3* is due to their near-zero values). This was probably due to the very similar turbulent flame speed throughout the combustion period, as seen in Fig. 2c. On a different note, the fluctuations seen in the AHRR and turbulent flame speed presented in Figs. 2b and 2c, and also in the rest of the figures in this paper, were probably due to the size of the global mesh.

The differences seen in Figs. 2a and 2b between the experiment data and simulations results are attributed to the use of a homogeneous

fuel and air charge versus stratified (GDI) gas mixture, reduced fuel chemistry, constant boundary conditions, and sub-models' uncertainties. However, Table 3 shows that differences were small. More, as simulation results not only matched the experiment, but were matching each other, too, it supports our hypothesis that different sets of C_{ms} and C_{m2} constants (which control the early flame development) can produce similar results.

Tuning Constant Effects

Understanding the C_{m2} and C_{ms} individual effect on the turbulent can help explain the predicted changes in the combustion behavior for different C_{m2}-C_{ms} sets. Figure 3 shows the effect that increasing one of the tuning variables while keeping the other constant had on the in-cylinder pressure. It was interesting to see that increasing C_{m2} (i.e., accelerating the transition to a fully developed turbulent flame) or decreasing C_{ms} (reducing the flame stretch) over the range of values investigated in this study (1.5 to 2.5 and 1 to 0 for C_{m2} and C_{ms}, respectively), while keeping the other tuning parameter constant, produced similar results. For example, the red solid and red dashed lines (i.e., two simulations that used C_{m2} and C_{ms} upper range values, 2.5 and 1.0, and lower range values for C_{ms} and C_{m2}, 1.5 and 0.0) or the green solid and green dashed lines (i.e., two simulations that used C_{m2} and C_{ms} of 1.8 and 1.0, and 1.5 and 0.5) show similar in-cylinder pressure traces.

The flame inception images shown in Figure 4 help to better understand the individual effects of C_{m2} and C_{ms}. For example, decreasing C_{m2} at constant C_{ms} accelerated the transition to fully development turbulent flame, but reduced the flame propagation. However, decreasing C_{ms} at constant C_{m2} increased the time for spark inception, but increased the flame propagation.

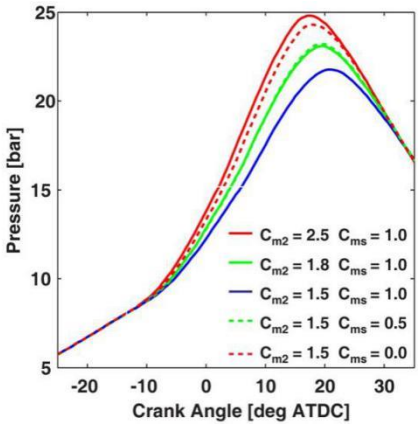

Figure 3. In-cylinder pressure for different sets of tuning constants. Solid lines show predictions made for increased C_{m2} at constant C_{ms}, while dashed lines showed predictions made for increased C_{ms} at constant C_{m2}. The transition from DPIK to G-equation was at -19 CAD ATDC.

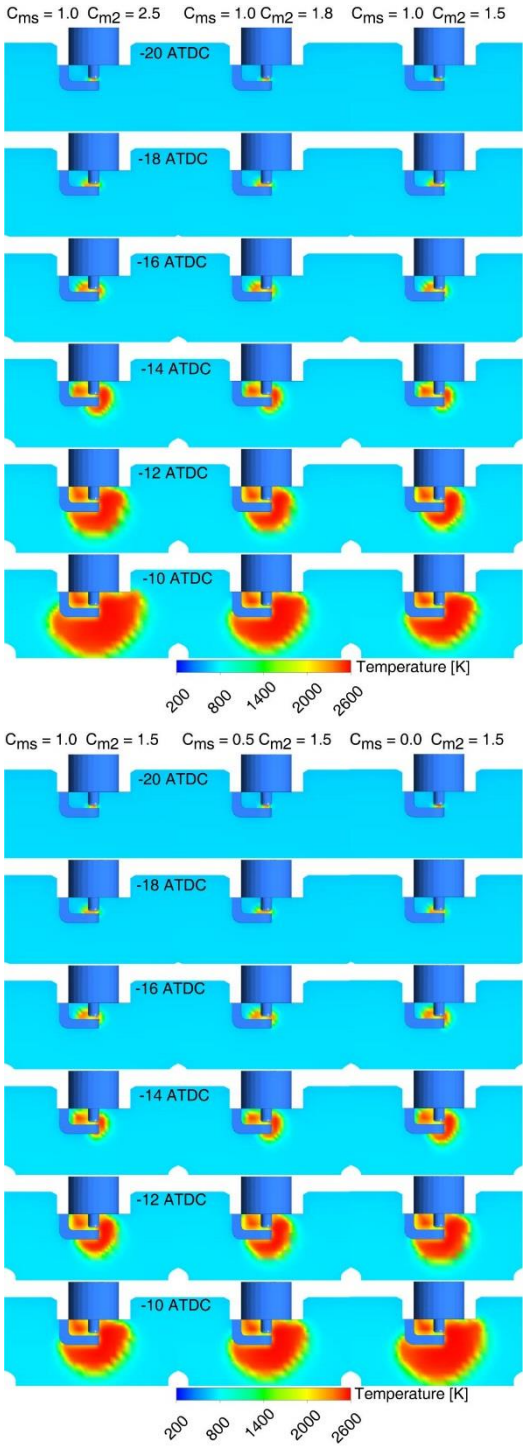

Figure 4. Effects of decreasing C_{m2} (top figure) and C_{ms} (bottom figure) on early flame development.

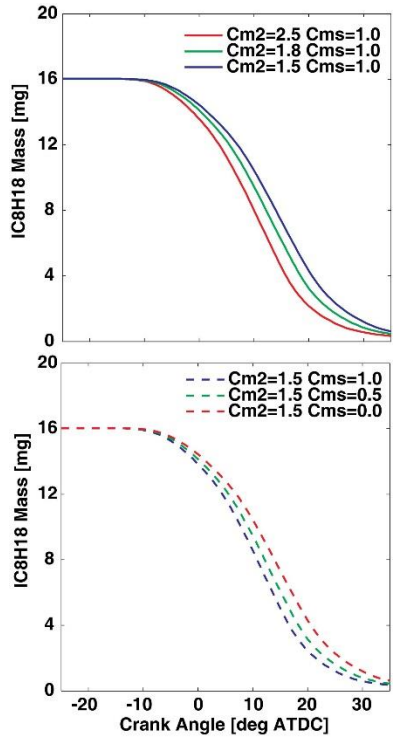

Figure 5. Effects of decreasing C_{m2} (top figure) and C_{ms} (bottom figure) on fuel mass burned.

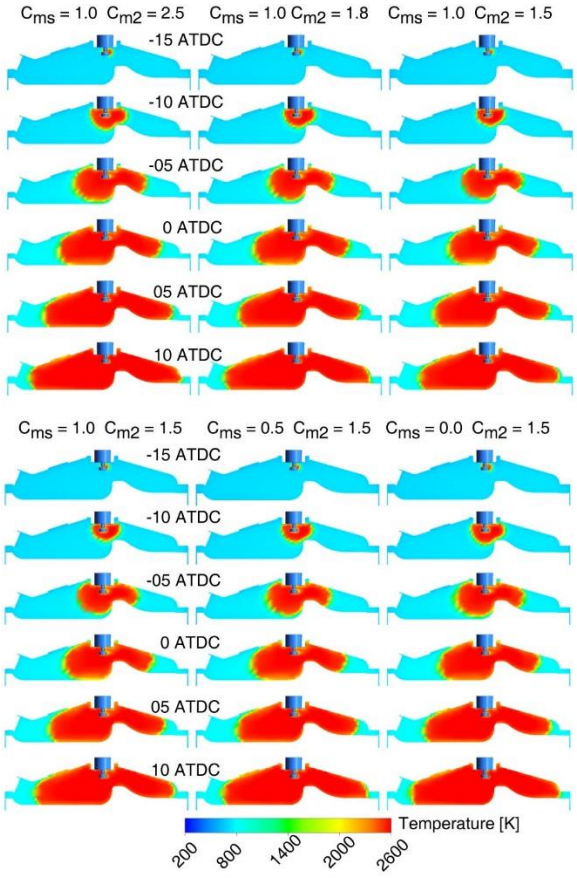

Figure 6. Flame propagation with decreasing C_{m2} and C_{ms} individually

It is also interesting to visualize in Figure 5 the effects of the early frame propagation due to the changes in either C_{m2} and C_{ms} on fuel mass burned. Figure 5 shows large changes in the fuel mass burned, particularly from mid-to-late combustion stages, which explains the large increase in the peak pressure seen in Figure 3. Figure 6 shows the turbulent flame propagation from -15 to -10 CAD ATDC. Again, the effects of the decrease in either C_{m2} and C_{ms} can be seen by comparing the flame size and reach at a specific crank angle. However, Figure 6 also shows that the two C_{m2}-C_{ms} pairs used for comparison ($C_{m2} = 2.5, C_{ms} = 1.0$ vs $C_{m2} = 1.5, C_{ms} = 0.0$)and ($C_{m2} = 1.8, C_{ms} = 1.0$ vs $C_{m2} = 1.5, C_{ms} = 0.5$) have almost identical flame propagation. The next sections will show if, in the absence of additional experimental data that will allow retuning, the predictions similarities are maintained when the operating conditions are changed.

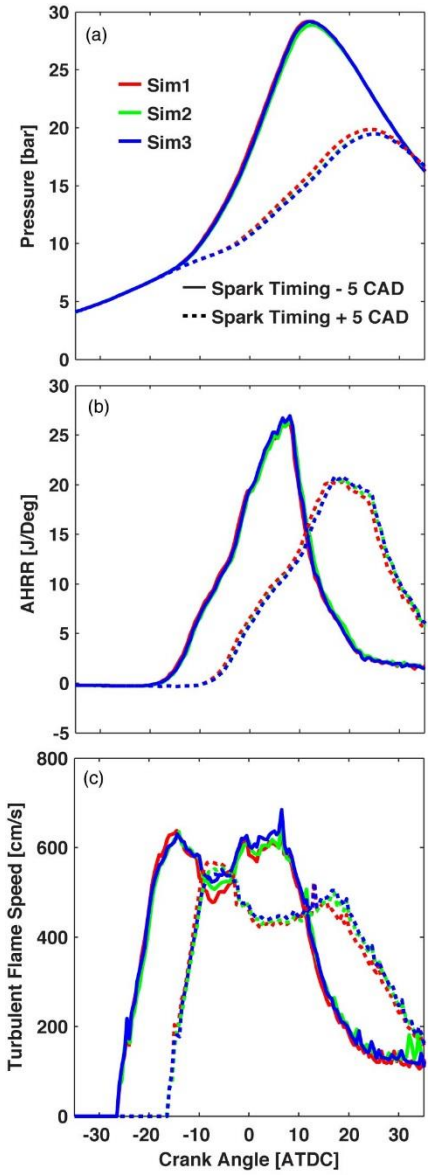

Figure 7. Pressure trace, apparent heat release rate (AHRR), and turbulent flame speed for numerical simulations with modified spark timing. Solid and dotted lines show an advanced or retarded sparking timing by 5 CAD, respectively. The transition from DPIK to G-equation for advanced and retarded spark timing cases was at -24 and -14 CAD ATDC, respectively.

Spark Timing Effects

This section presents simulation results when the spark timing (ST) for *Sim1*, *Sim2*, and *Sim3* was advanced or retarded by 5 CAD compared to the experiment's ST. Figure 7 shows the expected effect that ST has on the in-cylinder pressure, AHRR, or turbulent flame speed. Advanced ST increased the peak pressure and heat release rate, and reduced the combustion duration. Figure 7a shows that advanced ST also decreased the pressure gap between the simulations compared to the pressure traces shown in Fig. 2a. More, Figs. 7b shows very similar heat release rate for all three simulations at a particular ST, which suggests similar efficiency. This is probably due to the very similar turbulent flame speed, as seen in Fig. 7c, which suggests a very similar flame propagation.

Tables 5 and 6 show the main combustion parameters for the numerical simulations with advanced and retarded ST, respectively. As expected, the similar pressure trace, heat release rate and turbulent flame speed resulted in similar combustion parameters like peak pressure and its location, bulk temperature, start and duration of combustion, and thermal efficiency. However, there were some differences in the predicted emissions, particularly the HC emissions. This is probably due to variations in local flame speed close to the walls or towards the end of combustion, which are not captured the bulk averaged turbulent flame speed shown in Figure 7c. As a result, the actual values used for the C_{m2}-C_{ms} set seems to be important for emissions predictions. However, the HC emissions, particularly for the advanced ST, are close to zero, so it is difficult to say at this time how much of the difference is due to the C_{m2}-C_{ms} set or is just due to the numerical rounding throughout the simulation. More, as already mentioned, the chemistry did not include NO_x formation, so the effect on NO_x emissions is unknown.

Table 5. Main combustion parameters for the numerical simulations with advanced (-5 CAD) spark timing. The percentages indicate the change from *Sim1*.

Simulation #	*Sim1*	*Sim2*	*Sim3*
IMEP [bar]	5.3	+ 0.11%	+ 0.14%
Maximum Pressure [bar]	29.2	- 1.1%	- 0.15%
Max-Pressure Location [CA]	12.01	12.53	12.05
Maximum Temp [K]	2446	- 0.2%	+ 0.1%
Max-Temp Location [CA]	19.5	19.5	19.6
CA10 [CA ATDC]	-6.9	-6.4	-6.5
CA50 [CA ATDC]	5.0	5.6	5.0
CA90 [CA ATDC]	21.6	22.0	21.5
Combustion Duration [Deg]	28.5	28.4	28.0
Indicated η_{th} [%]	37.5%	+ 0.1%	+ 0.1%
CO Emission [g/kW-hr]	14.0	- 2.0%	- 0.8%
HC Emission [g/kW-hr]	0.003	- 17.9%	- 39.4%

Table 6. Main combustion parameters for the numerical simulations with delayed (+5 CAD) spark timing. The percentages indicate the change from *Sim1*.

Simulation #	*Sim1*	*Sim2*	*Sim3*
IMEP [bar]	5.0	- 0.52%	- 0.45%
Maximum Pressure [bar]	19.9	- 1.91%	- 1.93%
Max-Pressure Location [CA]	24.6	25.0	25.1
Maximum Temp [K]	2315	- 0.02%	+ 0.13%
Max-Temp Location [CA]	35.1	35.5	35.5
CA10 [CA ATDC]	3.6	4.0	4.1
CA50 [CA ATDC]	18.1	18.6	18.6
CA90 [CA ATDC]	34.0	34.1	34.1
Combustion Duration [Deg]	30.4	30.1	30.0
Indicated η_{th} [%]	35.7%	- 0.53%	- 0.45%
CO Emission [g/kW-hr]	14.9	+ 1.39%	+ 1.19%
HC Emission [g/kW-hr]	0.039	- 39.87%	- 55.32%

Engine Load Effects

The simulation results when the engine load for *Sim1*, *Sim2*, and *Sim3* was reduced by 50% (solid lines) or increased by 100% (dashed lines) are presented next. Figures 8a and 8b show almost identical pressure traces and AHRR for reduced load conditions, but there are some differences at the higher load conditions. Specifically, *Sim1* (i.e., the one using C_{m2} and C_{ms} upper range values) had a slightly higher and more advanced peak pressure and AHRR, compared to

Table 7. Main combustion parameters for the numerical simulations at 50% lower engine load. The percentages indicate the change from *Sim1*.

Simulation #	*Sim1*	*Sim2*	*Sim3*
IMEP [bar]	2.6	+ 0.17%	+ 0.15%
Maximum Pressure [bar]	13.5	+ 1.5%	+ 0.8%
Max-Pressure Location [CA]	15.0	14.5	14.5
Maximum Temp [K]	2257	+ 0.3%	+ 0.2%
Max-Temp Location [CA]	23.0	22.6	23.0
CA10 [CA ATDC]	-3.5	-3.4	-3.4
CA50 [CA ATDC]	8.5	8.1	8.5
CA90 [CA ATDC]	23.6	22.6	23.0
Combustion Duration [Deg]	27.1	26.0	26.4
Indicated η_{th} [%]	36.8%	+ 0.19%	+ 0.16%
CO Emission [g/kW-hr]	13.8	+ 0.39%	+ 1.27%
HC Emission [g/kW-hr]	0.035	- 32.62%	- 59.77%

Table 8. Main combustion parameters for the numerical simulations at 100% higher engine load. The percentages indicate the change from *Sim1*.

Simulation #	*Sim1*	*Sim2*	*Sim3*
IMEP [bar]	10.6	- 0.04%	- 0.16%
Maximum Pressure [bar]	56.2	- 1.3%	- 2.3%
Max-Pressure Location [CA]	13.1	13.5	14.1
Maximum Temp [K]	2577	- 0.1%	- 0.3%
Max-Temp Location [CA]	19.0	19.5	20.0
CA10 [CA ATDC]	-3.9	-3.5	-3.0
CA50 [CA ATDC]	6.0	6.6	7.1
CA90 [CA ATDC]	22.1	22.5	22.6
Combustion Duration [Deg]	26.0	26.0	25.6
Indicated η_{th} [%]	37.7%	- 0.03%	- 0.2%
CO Emission [g/kW-hr]	14.5	+ 0.1%	+ 1.3%
HC Emission [g/kW-hr]	0.001	- 39.9%	- 46.7%

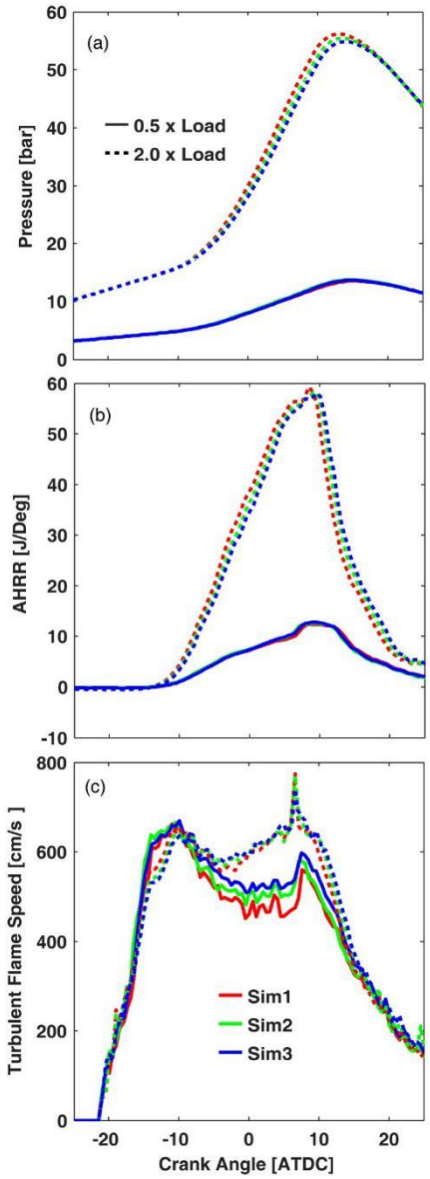

Figure 8. Pressure trace, apparent heat release rate (AHRR), and turbulent flame speed for numerical simulations with modified engine load. Solid and dotted lines show 0.5× and 2× the engine load, respectively. The transition from DPIK to G-equation for the lower and higher load cases was at -19.5 and -18.5 CAD ATDC, respectively.

Sim3 (i.e., the one using C_{m2} and C_{ms} lower range values). This is exact the opposite to the pressure and AHHR at 50% load conditions, shown in Figs. 8a and 8b. The effect that load had on the turbulent flame speed, seen in Fig. 8c, probably explains this behavior. *Sim1* had the larger flame stretch coefficient, C_{ms}, which reduces the turbulent flame speed for well-developed flame conditions, but also the highest flame development coefficient, C_{m2}, which accelerated the transition to a fully developed turbulent flame, compared to *Sim3*. As a result, at low load conditions (i.e., lower in-cylinder pressure and temperature), a higher flame development coefficient, C_{m2} could not compensate for the decreased flame stretch factor I_0 in Eq. 9, which reduced turbulent flame speed during the fast combustion period (i.e., between – 5 CAD and 10 CAD ATDC). However, the higher and more advanced peak pressure for *Sim 1* compared to *Sim2* and *Sim3* suggests that a faster transition to fully developed turbulent flame could compensate the slightly lower turbulent flame speed because the burning speed was at already high at higher loads (i.e., S_T is ~ 20% higher at 2× load compared to the 0.5× load conditions) during the fast combustion period. Therefore, load effects seem to depend on the C_{m2}-C_{ms} set used in the simulation, particularly at high load conditions. Tables 7 and 8 support this observation, with worth-mentioning differences seen only for the 100% load increase. However, even at high load the differences in thermal efficiency were negligible, smaller than those seen for spark timing effects.

Like the discussion around the ST effects, only HC emissions results were different between the three simulations. The difference is more important at lower load conditions, when the lower in-cylinder temperature is expected to affect more the fuel oxidation process. The higher load showed a similar large difference between the HC emissions, but as these emissions were almost zero, it is again difficult to reach a conclusion.

Engine Speed Effects

The last section presents the effect that the C_{m2}-C_{ms} set used in the simulation has on the combustion phenomena predictions when the engine speed is decreased by 50% (solid lines) or increased by 100%

Table 9. Main combustion parameters for the numerical simulations at 50% lower engine speed. The percentages indicate the change from Sim1.

	Sim1	*Sim2*	*Sim3*
IMEP [bar]	4.9	+ 0.11%	+ 0.07%
Maximum Pressure [bar]	29.9	- 2.4%	- 2.2%
Max-Pressure Location [CA]	10.0	11.0	11.0
Maximum Temp [K]	2409	- 0.5%	- 0.4%
Max-Temp Location [CA]	15.5	17.0	16.5
CA10 [CA ATDC]	-7.0	-6.0	-6.4
CA50 [CA ATDC]	2.5	3.5	3.5
CA90 [CA ATDC]	15.5	16.5	16.5
Combustion Duration [Deg]	22.5	22.5	22.9
Indicated η_{th} [%]	35.1%	+ 0.1%	+ 0.1%
CO Emission [g/kW-hr]	10.8	+ 1.0%	+ 0.9%
HC Emission [g/kW-hr]	0.002	- 1.3%	+ 48.0%

Table 10. Main combustion parameters for the numerical simulations at 100% higher engine speed. The percentages indicate the change from *Sim1*.

Simulation #	*Sim1*	*Sim2*	*Sim3*
IMEP [bar]	4.3	+ 5.02%	+ 10.95%
Maximum Pressure [bar]	12.7	+ 9.82%	+ 29.13%
Max-Pressure Location [CA]	20.6	27.1	27.6
Maximum Temp [K]	2162	+ 1.3%	+ 4.6%
Max-Temp Location [CA]	62.2	55.2	43.7
CA10 [CA ATDC]	8.2	6.7	5.0
CA50 [CA ATDC]	32.2	28.1	23.5
CA90 [CA ATDC]	58.6	53.5	46.0
Combustion Duration [CAD]	50.4	56.8	41.0
Indicated η_{th} [%]	30.6%	+ 5.0%	+ 11.0%
CO Emission [g/kW-hr]	22.2	- 8.6%	- 14.7%
HC Emission [g/kW-hr]	1.27	- 29.6%	- 67.6%

(dashed lines). The intake and exhaust manifolds are modeled; therefore, the simulation predicted the effect that speed has on the in-cylinder turbulence without the need to change any other simulation parameters or constants except the C_{m2}-C_{ms} set. Figure 9 and Table 9 show almost identical pressure traces, AHRR, and turbulent flame speed, and combustion characteristics, respectively, for the reduced speed conditions. This can be attributed to speed affecting both in-cylinder turbulence before the start of combustion (i.e., in-cylinder turbulence increases with increasing engine speed) and the time available for flame kernel growth and transition to turbulent flame (i.e., higher time at optimum flame development conditions at lower speed), which in turn affects more flame behavior than the change in tuning constants. However, a dramatic shift was observed when engine speed was doubled. As seen in Figure 9 and Table 10, the combustion phasing changed a lot at higher engine speed. The reason

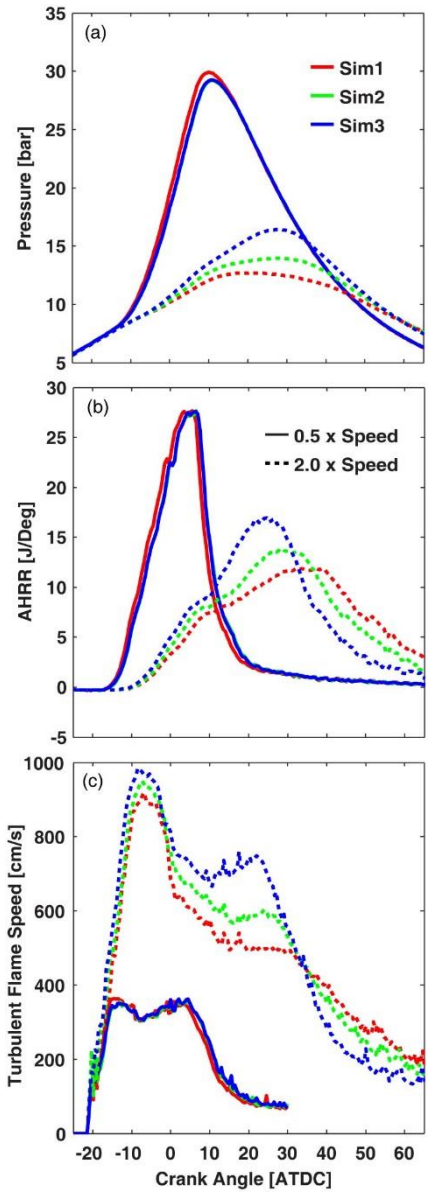

Figure 9. Pressure trace, apparent heat release rate (AHRR), and turbulent flame speed for numerical simulations with modified engine speed. Solid and dotted lines show 0.5× and 2× the engine speed, respectively. The transition from DPIK to G-equation for lower and higher engine speed was at -20 and -17 CAD ATDC, respectively.

was that while a real engine controller would advance the spark timing with increasing speed to maintain an optimum combustion phasing, the simulations shown here maintained a constant spark timing regardless of engine speed. However, the combustion phasing does not influence the effects of the tuning constants on simulation results as much as the in-cylinder flow motion affects. To check this assumption, simulations at a more advanced combustion phasing were run. The results were similar, with only emissions differences being slightly affected by the change in combustion phasing. As a result, the effect of combustion phasing was not considered here. The large differences in peak pressure, AHHR, and turbulent flame speed, and combustion characteristics during the fast combustion at higher engine speeds seen in Figure 9 and Table 10, respectively, suggest that the flame stretch coefficient, C_{ms}, has a much larger influence compared to the flame development coefficient, C_{m2}. As the spark timing was not advanced to optimize the combustion process at higher engine speed, most of the combustion took place late in the expansion stroke. As a result, a higher turbulent flame speed between TDC and 25 CAD ATDC ensured a higher burning rate under more optimum in-cylinder conditions (i.e., higher in-cylinder pressure and temperature), hence the higher peak pressure and heat release rates. The combustion duration also shortens by ~ 10 CAD from *Sim1* to *Sim3*.

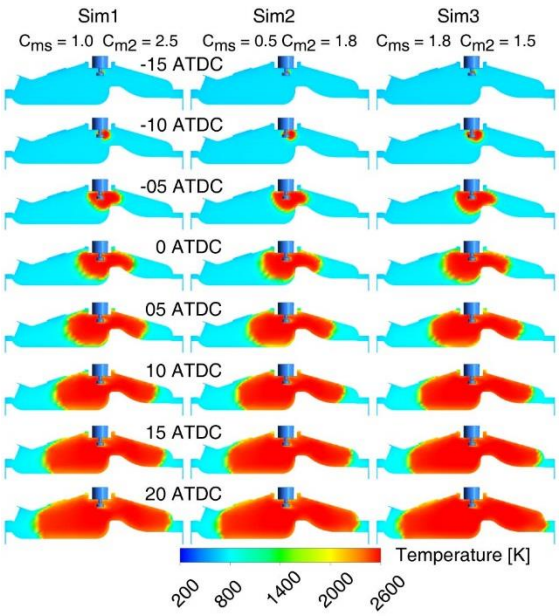

Figure 10. Flame propagation for numerical simulations at 2x engine speed.

The effects of increased turbulence at higher engine speed are also captured in Figure 10, which shows different flame propagation between the three simulations, with *Sim3* already showing a larger flame front at -10 CAD ATDC compared with *Sim1* and *Sim2*. This is better explained by large increase in flow velocity with speed seen in Figure 11. The maximum flow velocities inside the combustion chamber for a spark timing of -23 CAD ATDC and at 0.5x, 1x, and 2x engine speed were 3.5 m/s, 7 m/s, and 11.2 m/s, respectively, which suggests a highly turbulent environment at 2x engine speed compared to 0.5x speed. Of interest to early flame development is the large increase in flow velocity around the spark plug location, which greatly influence the early flame development, hence the large changes in peak pressure and phasing between simulations at the higher engine speed. In addition, not only that the flow velocity increases with speed, but also the turbulent kinetic energy and dissipation rate were affected by engine speed. Figure 12 shows a

larger increase in dissipation rate just before the spark timing for the 2x speed condition compared to both 0.5x and 1x speed operation, which help explain why there is a larger change between the three simulations at the higher speed.

In conclusion, the actual values for the C_{m2}-C_{ms} set seem to have the highest effect on higher engine speed changes.

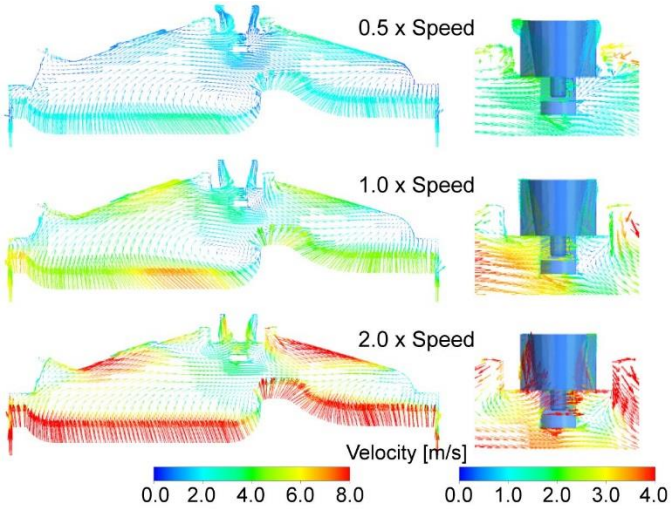

Figure 11. In-cylinder velocities at spark timing (-23 CAD ATDC), throughout the chamber (left side) and around the spark plug location (right side).

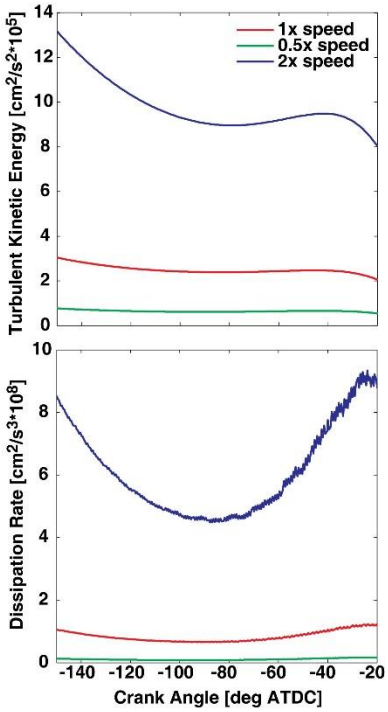

Figure 12. Turbulent kinetic energy and dissipation rate as function of the engine speed.

Summary/Conclusions

This study used ANSYS® Forte, Version 17.2, a CFD software package specifically designed for IC engines simulation, and its built-in G-equation-based premixed turbulent combustion model to investigate two tuning constants in G-equation that influence flame propagation in 3D CFD SI engine simulations: the stretch factor coefficient, C_{ms} and the flame development coefficient, C_{m2}. The model was validated with data from engine experiments performed in a 2.0-L GDI engine at Oak Ridge National Laboratory's National Transportation Research Center.

First, the study identified several sets of these two tuning coefficients that would allow the G-equation-based 3D CFD simulation to match experimental data at one operating condition. Then this work investigated how close the predictions made by each set were one to another when engine operating conditions such as speed, load, or spark timing were changed. The objective was to test the hypothesis that one set of tuning constants can be used to predict different engine operating conditions without the need to modify the set. The major observations and conclusions of this study are:

- C_{m2} and C_{ms} both influenced the early flame propagation, which affected fully developed turbulent flame behavior. As a result, this study identified three C_{m2}-C_{ms} sets can predict similar engine performance at one operating condition.

- The engine models that used different C_{m2}-C_{ms} sets predicted similar in-cylinder pressure, AHRR, and turbulent flame speed, as well as similar start of combustion or combustion duration, when the spark timing, engine load, and engine speed were changed from the operating condition used to validate the CFD simulation.

- A dramatic shift was observed when engine speed was doubled. Simulation analysis suggested that the flame stretch coefficient, C_{ms}, had a much larger influence at higher engine speeds compared to the flame development coefficient, C_{m2}. As the spark timing was not advanced to optimize the combustion process at higher engine speed, most of the combustion took place late in the expansion stroke. Therefore, the C_{m2}-C_{ms} sets that predicted a higher turbulent flame speed between TDC and 25 CAD ATDC increased the burning rate under more optimum in-cylinder conditions (i.e., higher in-cylinder pressure and temperature), hence a large shift in higher peak pressure and heat release rates between the simulations. This suggest that the choice of the C_{m2}-C_{ms} will affect the simulation accuracy when engine speed increases from the one used to validate the model.

In conclusion, even if current phenomenological G-equation-based 3D CFD engine simulations combine complex sub-models with solution-adaptive mesh refinement and coarsening, and improved chemistry solvers, this study suggests that finding the set of constants that can be used to predict different engine operating conditions without the need to modify the set is not trivial. In addition, the G-equation-based 3D CFD simulation needs enough experimental data for validation at very different conditions. As a result, for the less-experimented CFD user and in the absence of enough experimental data that would help retune the tuning parameters at various operating conditions, the purpose of a good G-equation-based 3D engine simulation is to guide and/or complement experimental investigations, not the other way around. Only a truly-predictive simulation that fully couples the turbulence/chemistry equations can help reduce the amount of experimental work.

References

1. Hessel, R., Reitz, R., Yue, Z., Musculus, M. et al., "Applying Advanced CFD Analysis Tools to Study Differences between Start-of-Main and Start-of-Post Injection Flow, Temperature and Chemistry Fields Due to Combustion of Main-Injected Fuel," SAE Int. J. Engines 8(5):2159-2176, 2015, https://doi.org/10.4271/2015-24-2436.
2. Bartolucci, L., Cordiner, S., Mulone, V., Rocco, V. et al., "Partially Stratified Charge Natural Gas Combustion: A LES Numerical Analysis," SAE Technical Paper 2015-01-0398, 2015, https://doi.org/10.4271/2015-01-0398.
3. ANSYS®, "Academic Research Mechanical and CFD, Release 17.2."
4. Convergent Science, "Converge CFD."
5. OpenCFD Ltd, "Openfoam®."
6. Verma, I., Bish, E., Kuntz, M., Meeks, E. et al., "CFD Modeling of Spark Ignited Gasoline Engines- Part 1: Modeling the Engine under Motored and Premixed-Charge Combustion Mode," SAE Technical Paper 2016-01-0591, 2016, https://doi.org/10.4271/2016-01-0591.
7. Verma, I., Bish, E., Kuntz, M., Meeks, E. et al., "CFD Modeling of Spark Ignited Gasoline Engines- Part 2: Modeling the Engine in Direct Injection Mode along with Spray Validation," SAE Technical Paper 2016-01-0579, 2016, https://doi.org/10.4271/2016-01-0579.
8. McNenly, Matthew J., Russell A. Whitesides, and Daniel L. Flowers. "Faster solvers for large kinetic mechanisms using adaptive preconditioners." Proceedings of the Combustion Institute 35, no. 1 (2015): 581-587, https://doi.org/10.1016/j.proci.2014.05.113.
9. Ra, Youngchul, and Rolf D. Reitz. "A combustion model for IC engine combustion simulations with multi-component fuels." Combustion and flame 158, no. 1 (2011): 69-90, https://doi.org/10.1016/j.combustflame.2010.07.019.
10. Williams, F. A. "3. Turbulent combustion", in "The mathematics of combustion", J. Buckmaster, ed., pp. 97-131.
11. ANSYS® Forte, Release 17.2, "User Guide", Ansys, Inc.
12. Peters, N. "Turbulent Combustion Cambridge University Press." Cambridge, UK (2000).
13. Liang, Long, Rolf D. Reitz, Jianwen Yi, and Claudia O. Iyer. "A G-equation combustion model incorporating detailed chemical kinetics for PFI/DI SI engine simulations." In SAE Congress April, vol. 2. 2006.
14. Liang, L., Reitz, R., Iyer, C., and Yi, J., "Modeling Knock in Spark-Ignition Engines Using a G-equation Combustion Model Incorporating Detailed Chemical Kinetics," SAE Technical Paper 2007-01-0165, 2007, https://doi.org/10.4271/2007-01-0165.
15. Tan, Zhichao, and Rolf D. Reitz. "An ignition and combustion model based on the level-set method for spark ignition engine multidimensional modeling." Combustion and flame 145, no. 1 (2006): 1-15, https://doi.org/10.1016/j.combustflame.2005.12.007.
16. Tan, Z., Kong, S., and Reitz, R., "Modeling Premixed and Direct Injection SI Engine Combustion Using the G-Equation Model," SAE Technical Paper 2003-01-1843, 2003, https://doi.org/10.4271/2003-01-1843.
17. Liang, L. and Reitz, R., "Spark Ignition Engine Combustion Modeling Using a Level Set Method with Detailed Chemistry," SAE Technical Paper 2006-01-0243, 2006, https://doi.org/10.4271/2006-01-0243.
18. Metghalchi, Mohamad, and James C. Keck. "Burning velocities of mixtures of air with methanol, isooctane, and indolene at high pressure and temperature." Combustion and flame 48 (1982): 191-210, https://doi.org/10.1016/0010-2180(82)90127-4.
19. Gülder, Ömer L. "Laminar burning velocities of methanol, ethanol and isooctane-air mixtures." In Symposium (international) on combustion, vol. 19, no. 1, pp. 275-281. Elsevier, 1982, https://doi.org/10.1016/S0082-0784(82)80198-7.
20. Fan, L., Li, G., Han, Z., and Reitz, R., "Modeling Fuel Preparation and Stratified Combustion in a Gasoline Direct Injection Engine," SAE Technical Paper 1999-01-0175, 1999, https://doi.org/10.4271/1999-01-0175.
21. Tan, Zhichao. "Multi-dimensional modeling of ignition and combustion in premixed and DIS/CI (direct injection spark/compression ignition) engines." (2004): 4008-4008.
22. Herweg, R. and Maly, R., "A Fundamental Model for Flame Kernel Formation in S. I. Engines," SAE Technical Paper 922243, 1992, https://doi.org/10.4271/922243.
23. Han, Zhiyu, and Rolf D. Reitz. "Turbulence modeling of internal combustion engines using RNG κ - ε models." Combustion science and technology 106, no. 4-6 (1995): 267-295, http://dx.doi.org/10.1080/00102209508907782.
24. Chang, Y., and Szybist, J., "Fuel Effects on Combustion with EGR Dilution in Spark Ignited Engines," Proceedings of the 2016 Central States Meeting of the Combustion Institute, Paper No. 145IC-0082.
25. Matsumoto, A., Zheng, Y., Xie, X., Lai, M. et al., "Characterization of Multi-hole Spray and Mixing of Ethanol and Gasoline Fuels under DI Engine Conditions," SAE Technical Paper 2010-01-2151, 2010, https://doi.org/10.4271/2010-01-2151.
26. Matsumoto, A., Zheng, Y., Xie, X., Lai, M. et al., "Interactions of Multi-hole DI Sprays with Charge Motion and their Implications to Flexible Valve-trained Engine Performance," SAE Technical Paper 2011-01-1883, 2011, https://doi.org/10.4271/2011-01-1883.
27. Mehl, Marco, Jyh-Yuan Chen, William J. Pitz, S. Mani Sarathy, and Charles K. Westbrook. "An approach for formulating surrogates for gasoline with application toward a reduced surrogate mechanism for CFD engine modeling." Energy & Fuels 25, no. 11 (2011): 5215-5223, https://doi.org/10.1021/ef201099y.
28. Mehl, Marco, William J. Pitz, Charles K. Westbrook, and Henry J. Curran. "Kinetic modeling of gasoline surrogate components and mixtures under engine conditions." Proceedings of the Combustion Institute 33, no. 1 (2011): 193-200, https://doi.org/10.1016/j.proci.2010.05.027.
29. Yakhot, Victor, and Steven A. Orszag. "Renormalization group analysis of turbulence. I. Basic theory." Journal of scientific computing 1, no. 1 (1986): 3-51, https://doi.org/10.1007/BF01061452.

Contact Information

Corresponding author: Cosmin E. Dumitrescu
West Virginia University, P.O. Box 6106, Morgantown, WV 26506, USA; tel.: 304-293-3330; fax: 304-293-6689; e-mail address: cosmin.dumitrescu@mail.wvu.edu

Acknowledgments

This work was funded by the US Department of Energy's Office of Vehicle Technologies under the guidance of the Advanced

Combustion Engines and Systems program managed by Gurpreet Singh and Michael Weismiller. The CFD investigation and preparation of this manuscript was funded by West Virginia University and the Ralph E. Powe Junior Faculty Enhancement Award. The authors gratefully acknowledge the support of the Oak Ridge National Laboratory's National Transportation Research Center (many thanks to Dr.K. Dean Edwards for his valuable review and suggestions) and ANSYS®/Reaction Design® to this research.

The simulations were performed on the Super Computing System (Mountaineer) at WVU, which is funded in part by the National Science Foundation EPSCoR Research Infrastructure Improvement Cooperative Agreement #1003907, the state of West Virginia (WVEPSCoR via the Higher Education Policy Commission) and WVU.

Definitions/Abbreviations

3D	Three Dimensional
b_1	Turbulent Flame Speed Ratio
C_{m2}	Flame Development Coefficient
C_{ms}	Stretch Factor Coefficient
AHRR	Apparent Heat Release Rate
ATDC	After Top Dead Center
BTDC	Before Top Dead Center
CAx	CAD Corresponding to x % Mass Fraction Burned
CAD	Crank Angle Degree
CFD	Computational Fluid Dynamics
DPIK	Discrete Particle Ignition Kernel
EOC	End of Combustion
GDI	Gasoline Direct Injection
IC	Internal Combustion
IMEP	Indicated Mean Effective Pressure
RANS	Reynolds Averaged Navier-Stokes
RHS	Right Hand Side
RNG	Re-Normalization Group
SI	Spark Ignition
SOC	Start of Combustion
SOI	Start of Injection
TDC	Top Dead Center